*Int. J. Heat Mass Transfer.* Vol. 28, No. 2, pp. 485–495, 1985
Printed in Great Britain

0017-9310/85 $3.00 + 0.00


# Heat transfer in porous media considering phase change and capillarity—the heat pipe effect

KENT S. UDELL
Department of Mechanical Engineering, University of California, Berkeley, CA 94720, U.S.A.

(*Received* 6 *September* 1983; *and in revised form* 18 *July* 1984)

**Abstract**—A one-dimensional, steady state analysis of the heat and mass transfer in porous media saturated with the liquid and vapor phases of a single component fluid was conducted. The effects of capillarity, gravity forces, and phase change were included. Theoretical results were compared to experimental data with excellent agreement. It was found that the heat transfer was increased several orders of magnitude beyond pure conduction due to an evaporation, convection and condensation phenomenon similar to conventional heat pipe operation. The dry-out heat flux was predicted and verified for the bottom heating orientation. Theoretical temperature, pressure and saturation profiles within the two-phase region were obtained. Apparent thermal conductivities were evaluated for various gravitational orientations and medium permeabilities

## 1. INTRODUCTION

A WIDE variety of industrial, agricultural and energy production processes involve heat and mass transfer in porous media saturated with multiple fluid phases. In many such systems, the interstitial fluids are subject to vaporization, condensation and transport due to pressure, temperature, or concentration gradients. Examples include the drying of porous solids and soils, geothermal energy production, thermally enhanced oil recovery, underground high-level nuclear waste disposal, heat transfer from buried pipelines and electrical cables, heat pipe wicks, and post-accident boiling of fluids within nuclear reactor debris. The inherent difficulties in the evaluation of the heat transfer in such systems result from the lack of understanding of multiphase interactions which are unique to porous media. For the majority of porous materials of interest, the pore dimensions are small, which accentuates the interfacial tension effects and presents experimental difficulties in obtaining data on system variables such as individual phase pressures, liquid–vapor interfacial geometry, and fluid velocities on the pore level. Furthermore, the pore geometry is extremely complex requiring macroscopic averaging of microscopic phenomena. Nevertheless, the quantitative evaluation of the heat and mass transfer characteristics of porous media with fluid phase change is possible through the theoretical and experimental study of well-defined systems. This paper presents such a study. The analysis will be restricted to a one-dimensional, steady state problem in which a temperature difference is applied across a slab of porous material saturated with the liquid and vapor phases of a single component fluid. Gravity, capillarity, multiphase flow, and phase change effects are included.

Other researchers have studied heat transfer in porous media with phase change. Early work has been reported by soil science researchers [1–4]. A summary of Soviet research in modelling heat and mass transfer in capillary-porous media was published by Luikov [5]. Theoretical and experimental work was performed by Krischer [6] in Germany. Other analytic studies of the effects of phase change on energy and mass transport have been reported by Sahota and Pagni [7], Eckert and Faghri [8], and Ogniewicz and Tien [9, 10]. The above list of work is not an extensive review of the literature but a selected number of major contributions in the modelling of heat and mass transfer in unsaturated porous media.

Experimental studies have also been reported. Hansen, Breyer and Riback [11] conducted bottom heating experiments with glass and copper beads saturated with air and water. Their results showed an enhancement of the heat transfer over that of conduction in water saturated porous media due to the convective contributions of the water and vapor phases. Gomaa and Somerton [12] also obtained effective thermal conductivity data on steam–water saturated porous materials which were several times larger than those of the same medium saturated only with the liquid phase. They postulated that the dominant heat transfer mechanism in their experiments was condensation, capillary movement of the liquid, and revaporization, which is analogous to the phenomena of a heat pipe. Su [13] conducted experiments to isolate the two-phase zone from the liquid or vapor saturated zones. Other researchers have heated confined water saturated porous media from the bottom [14, 15], the side [16] and internally [17], all producing a two-phase, heat pipe zone which was nearly isothermal and convection dominated. Similar experimental studies conducted on heat pipe wicks to determine dry-out conditions are available in the literature [18–20].

In a recent study by this author [21], water saturated sand was heated from above, which permitted determination of the significance of capillarity. A model was developed to predict the length

## NOMENCLATURE

| | |
|---|---|
| $f$ | non-dimensional capillary pressure |
| $f'$ | $df/ds$ |
| $g$ | gravitational constant |
| $h_{fg}$ | latent heat of evaporation |
| $k$ | thermal conductivity |
| $k_{app}$ | apparent thermal conductivity |
| $\dot{m}$ | mass flux |
| $\bar{P}$ | non-dimensional pressure |
| $P$ | pressure |
| $P_c$ | capillary pressure |
| $P^*$ | saturation pressure in the two-phase zone |
| $P_0$ | saturation pressure at the interface between the liquid zone and two-phase zone |
| $q$ | heat flux |
| $R$ | gas constant |
| $s$ | scaled liquid saturation |
| $s_l$ | liquid saturation (volume fraction of pore occupied by the liquid phase) |
| $s_{lp}$ | saturation of immobile water |
| $T$ | temperature |
| $T_0$ | saturation temperature corresponding to $P_0$ |
| $v$ | fluid superficial velocity |
| $x$ | distance |
| $x_l$ | length of two-phase zone. |

Greek symbols

| | |
|---|---|
| $\beta$ | liquid/vapor kinematic viscosity ratio |
| $\delta$ | non-dimensional distance |
| $\delta_l$ | non-dimensional length of the two-phase zone |
| $\kappa$ | permeability |
| $\kappa_r$ | relative permeability |
| $\mu$ | fluid dynamic viscosity |
| $\nu$ | fluid kinematic viscosity |
| $\rho$ | fluid density |
| $\sigma$ | vapor–liquid interfacial tension |
| $\Phi$ | fluid potential |
| $\phi$ | porosity |
| $\psi$ | wick limit |
| $\omega$ | non-dimensional convective heat flux |
| $[\omega/\sin\theta]_{cr}$ | critical dry-out heat flux. |

Subscripts

| | |
|---|---|
| l | liquid phase |
| v | vapor phase. |

of this zone as a function of the heat flux, fluid properties, and porous medium characteristics. It was also shown that for thermodynamic equilibrium to exist between phases in such liquid-wetting media, the vapor must be slightly superheated as predicted by the Kelvin equation and the liquid will be in a stable superheated state due to interfacial tension effects.

As an extension of that previous work [21], this study evaluates saturation, pressure and temperature profiles corresponding to other gravitational orientations, and identifies conditions under which gravitational effects can be neglected. Criteria for determining the dry-out heat flux are established and apparent thermal conductivities of the two-phase zone are presented.

## 2. THEORETICAL FORMULATION

Consider the one-dimensional, steady-state problem of a fluid-filled porous media subjected to a temperature difference such that the temperature at the heated end is significantly above the saturation temperature of the interstitial fluid while the cooled end is maintained below the saturation temperature, as shown in Fig. 1. For porous media with small pore dimensions, it has been shown [21] that three distinct regions will appear in this system:

1. A conduction dominated zone at the heated end with the voids filled with superheated vapor.
2. A nearly isothermal two-phase convective zone dominated by countercurrent flow of liquid to the heated end and vapor to the cooled end, and
3. A conduction dominated, compressed liquid zone at the cooled end.

The quantitative description of the heat transfer through these three regions requires knowledge of the length of the two-phase transition zone, $x_1$, as a function of the heat flux, assuming that the thermal

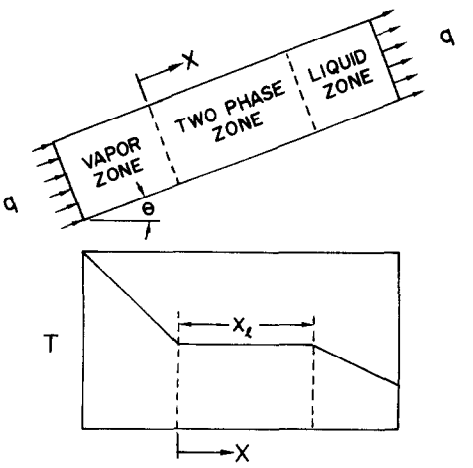


FIG. 1. System geometry and thermal characteristics.

conductivities of the liquid and vapor saturated zones are known. Thus, this problem reduces to the one-dimensional, steady state analysis of the heat and mass transfer within the two-phase zone. Several assumptions can be incorporated to simplify the solution without unduly restricting the results. These assumptions are listed below.

1. Temperature gradients within the two-phase zone are small.
2. The flow of both liquid and vapor phases are dominated by viscous forces and can be described by Darcy's Law.
3. The transport properties of the liquid and vapor are constant in the two-phase zone.
4. The evaporation and condensation processes occur in narrow regions which bound the two-phase zone.

The fundamental variables describing the counter-current flow of the vapor and liquid are the pressures in each phase. The mass fluxes of the liquid and vapor phases can be related to the pressure gradients through Darcy's equation, modified for two-phase flow:

$$\dot{m}_l = -\frac{\rho_l^2 \kappa \kappa_{rl}}{\mu_l}\frac{d\Phi_l}{dx} \tag{1}$$

$$\dot{m}_v = -\frac{\rho_v^2 \kappa \kappa_{rv}}{\mu_v}\frac{d\Phi_v}{dx} \tag{2}$$

where the fluid potential ($\Phi_{l,v}$) is defined by:

$$\Phi_{l,v} \equiv \frac{P_{l,v}}{\rho_{l,v}} + gx\sin\theta. \tag{3}$$

The variables $\kappa_{rl}$ and $\kappa_{rv}$ are the relative permeabilities of the liquid and vapor phases, respectively. The relative permeabilities are typically obtained experimentally and account for a decrease in the effective flow cross-section due to the presence of the other fluid.

Due to the interfacial tension forces, the pressure of the vapor phase will be greater than that of the liquid pressure for the liquid-wetting porous media considered in this analysis. The vapor–liquid pressure difference can be defined as the capillary pressure ($P_c$):

$$P_c = P_v - P_l. \tag{4}$$

The capillary pressure is directly proportional to the interfacial tension and inversely proportional to the effective meniscus radius of the vapor–liquid interface within a given pore.

The assumptions of negligible temperature gradients and constant properties in the two-phase zone allow reduction of the energy equation to the following expression:

$$q = \dot{m}_v h_{fg}. \tag{5}$$

At any location, mass conservation requires that the net mass flux be zero for steady-state conditions

$$\dot{m}_v + \dot{m}_l = 0. \tag{6}$$

By solving for the pressure gradients in (1) and (2) and incorporating (5) and (6), the following expressions for the vapor and liquid pressure gradients are obtained.

$$\frac{dP_v}{dx} = -\frac{v_v q}{h_{fg}\kappa\kappa_{rv}} - \rho_v g\sin\theta \tag{7}$$

$$\frac{dP_l}{dx} = +\frac{v_l q}{h_{fg}\kappa\kappa_{rl}} - \rho_l g\sin\theta. \tag{8}$$

The subtraction of equation (8) from equation (7) results in the capillary pressure gradient

$$\frac{dP_c}{dx} = -\frac{q}{\kappa h_{fg}}\left(\frac{v_v}{\kappa_{rv}} + \frac{v_l}{\kappa_{rl}}\right) + (\rho_l - \rho_v)g\sin\theta. \tag{9}$$

Leverett [22] has shown that capillary pressure versus saturation data can be cast in the following non-dimensional form

$$f(s) = \frac{P_c}{\sigma}\left(\frac{\kappa}{\phi}\right)^{1/2}. \tag{10}$$

Expression (10) implies that the characteristic pore dimension is proportional to $(\kappa/\phi)^{1/2}$. Capillary pressures for various low porosity ($\phi < 0.50$) media are well correlated by the use of (10) if the saturation is scaled by the following relation

$$s = \frac{s_l - s_{lp}}{1 - s_{lp}}. \tag{11}$$

The variable $s_{lp}$ is the saturation of the liquid in a pendular ring distribution within the porous medium. At this saturation, the liquid becomes immobile since no interpore connections of the liquid exist.

Through the use of (10), equation (9) can be rewritten in the following dimensionless form:

$$\frac{df}{d\delta} = \sin\theta - \omega\left(\frac{1}{\kappa_{rv}} + \frac{\beta}{\kappa_{rl}}\right) \tag{12}$$

where

$$\omega = \frac{q v_v}{\kappa h_{fg}(\rho_l - \rho_v)g}$$

$$\delta = \frac{x(\rho_l - \rho_v)g}{\sigma}\left(\frac{\kappa}{\phi}\right)^{1/2}$$

$$\beta = \frac{v_l}{v_v}.$$

The variable $\omega$ is the ratio of the vapor pressure gradient to the hydrostatic pressure gradient and $\delta$ results from scaling $x$ by the capillary suction height.

Since $f$ is a function of $s$ only, equation (12) can be written as:

$$\frac{df}{d\delta} = f'\frac{ds}{d\delta}. \tag{13}$$

By setting (13) equal to (14), and solving for the saturation gradient, the following first order differential equation results:

$$\frac{ds}{d\delta} = \frac{\sin\theta - \omega\left(\frac{1}{\kappa_{rv}} + \frac{\beta}{\kappa_{rl}}\right)}{f'}. \tag{14}$$

Since $\kappa_{rv}$, $\kappa_{rl}$ and $f'$ are functions only of $s$, equation (14) can be integrated directly if $\kappa_{rv}$, $\kappa_{rl}$ and $f'$ are specified. Thus, the liquid saturation profile can be obtained and the two-phase zone length ($\delta_l$) can be defined by imposing the limits of integration of $s = 0$ at $\delta = 0$ and $s = 1$ at $\delta = \delta_l$.

The thermal characteristics of the two-phase zone can be evaluated through the knowledge of the vapor and liquid pressure profiles, coupled with thermodynamic equations of state. The pressures can be referenced to the saturation pressure ($P_0$) and scaled by the characteristic capillary pressure to obtain the following non-dimensional pressures:

$$\bar{P}_v = \frac{(P_v - P_0)}{\sigma}\left(\frac{\kappa}{\phi}\right)^{1/2} \quad \text{and} \quad \bar{P}_l = \frac{(P_l - P_0)}{\sigma}\left(\frac{\kappa}{\phi}\right)^{1/2}.$$

Equations (7) and (8) can be non-dimensionalized and rewritten in the following forms, through the use of equation (14).

$$\frac{d\bar{P}_v}{ds} = \frac{-\omega f'/\kappa_{rv}}{\sin\theta - \omega\left(\frac{1}{\kappa_{rv}} + \frac{\beta}{\kappa_{rl}}\right)} \tag{15}$$

and

$$\frac{d\bar{P}_l}{ds} = \frac{wf'/\kappa_{rl} - f'\sin\theta}{\sin\theta - \omega\left(\frac{1}{\kappa_{rv}} + \frac{\beta}{\kappa_{rl}}\right)}. \tag{16}$$

Included in the derivation of (15) and (16) is the assumption that $\rho_v/\rho_l \ll 1$. The integration of (15) and (16) results in each phase pressure as a function of saturation. Thus, the pressure distributions are obtained through reference to the saturation profile obtained from the integration of (14).

Temperatures within the two-phase zone can be calculated from the vapor and liquid pressures. From the Kelvin equation, the local saturation pressure ($P^*$) corresponding to the temperature ($T$) can be expressed as a function of capillary pressure and vapor pressure by:

$$P^* = P_v \exp\left(\frac{P_c}{\rho_l RT}\right). \tag{17}$$

The Clapeyron equation, integrated under the assumptions of ideal gas behavior of the vapor phase and small liquid specific volume, yields the following:

$$P^* = P_0\, e^{(1/T_0 - 1/T)h_{fg}/R}. \tag{18}$$

The temperature as a function of vapor pressure and capillary pressure is derived from the combination of (17) and (18) and can be expressed as:

$$T = \frac{T_0(1 + P_c/h_f\rho_l)}{1 - T_0 R/h_{fg}\ln\dfrac{P_v}{P_0}}. \tag{19}$$

The reference saturation pressure ($P_0$) and temperature ($T_0$) are arbitrary but are defined in this work as the pressure and corresponding saturation temperature at $\delta = \delta_l$. At this location the capillary pressure is zero and the vapor pressure will equal the reference pressure.

Apparent thermal conductivities in the two-phase zone can be calculated directly by dividing the heat flux by the temperature gradient. The temperature gradient is obtained by the differentiation of equation (19) with respect to $x$ and will be a function of the capillary and vapor pressures, as well as their gradients, which have been expressed previously.

Three cases are of interest in this study: horizontal heating ($\theta = 0$), top heating ($0 > \theta > -\pi$), and bottom heating ($0 < \theta < \pi$). In order to quantify the results, the following functional forms of $f(s)$, $\kappa_{rv}(s)$ and $\kappa_{rl}(s)$ are assumed:

$$f = 1.417(1-s) - 2.120(1-s)^2 + 1.263(1-s)^3 \tag{20}$$

$$\kappa_{rl} = s^3 \tag{21}$$

$$\kappa_{rv} = (1-s)^3. \tag{22}$$

Equation (20) results from a correlation of imbibition capillary pressure data obtained by Leverett [22]. The liquid and vapor relative permeability data reported by Fatt and Klikoff [23] are well represented by equations (21) and (22), respectively. These forms of the relative permeabilities are also suggested by Wyllie [24].

### 2.1. *Horizontal heating*

Consideration of equation (14) for the case of $\sin\theta = 0$ yields two important results. First, equation (14) can be written in the following form:

$$\frac{ds}{d\delta} = \frac{\omega\left(\frac{1}{\kappa_{rv}} + \frac{\beta}{\kappa_{rl}}\right)}{-f'}. \tag{23}$$

Integrating (23), one obtains:

$$\omega\delta_l = \int_0^1 \frac{-f'}{\left(\frac{1}{\kappa_{rv}} + \frac{\beta}{\kappa_{rl}}\right)}\, ds. \tag{24}$$

Since all variables in the integrand are functions of $s$ only, the right-hand side of (24) is a constant for a given $\beta$. The integration of (18) was performed using a sixth-order Runge–Kutta algorithm, resulting in the following:

$$\frac{qx_l v_v}{(\kappa\phi)^{1/2} h_{fg}\sigma} = \psi(\beta). \tag{25}$$

The non-dimensional grouping on the left-hand side of (25) is identical to the non-dimensional heat pipe wick limit defined by Ogniewicz and Tien [10]. The function $\psi(\beta)$ is shown in Fig. 2 for $10^{-3} \leqslant \beta \leqslant 1$.

Second, through consideration of equations (23) and (24), it follows that the saturation profile, normalized with respect to $\delta_l$, is independent of the heat flux. Thus, the saturation is a similarity variable under conditions where gravity effects are negligible.

### 2.2. *Heating from above*

For the case of $\sin\theta < 0$, two limiting conditions can be identified from equation (16). For $|\omega/\sin\theta| \gg 1$, the second term in the numerator of the right-hand side of

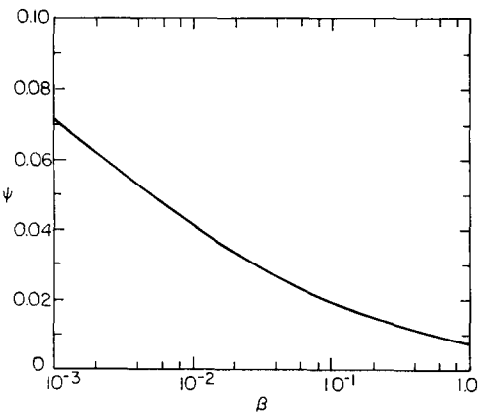


FIG. 2. Wick limit as a function of liquid/vapor kinematic viscosity ratio, $\beta$.

(16) dominates the first. Therefore, the high heat flux or low permeability cases reduce to results of horizontally heated media, equation (25).

Under the condition of $|\omega/\sin\theta| \ll 1$, the following can be written:

$$\sin\theta\delta_l = \int_0^1 f'\,ds. \tag{26}$$

Thus, the two-phase zone length is limited by the capillary suction height, $f(0)$, for low heat flux or high permeability systems heated from above.

### 2.3. *Bottom heating*

The case of $0 < \theta < \pi$ is of particular interest. For small values of $\omega/\sin\theta$, there is at least one value of $s$ $(0 < s < 1)$ for which the following results:

$$\sin\theta - \omega\left(\frac{1}{\kappa_{rv}} + \frac{\beta}{\kappa_{rl}}\right) = 0. \tag{27}$$

Under this condition, the sum of the liquid and vapor pressure gradients is equal to the hydrostatic pressure gradient. Therefore, the potential for fluid movement is provided through gravitational forces alone. As defined by equation (16), the saturation gradient is also equal to zero at this saturation and thus there is no theoretical limit to the length of the two-phase zone. The necessary, but not sufficient condition for a vapor zone to exist at the heated end is the absence of real roots of equation (27). This condition is met if $\omega/\sin\theta$ is greater than the critical heat flux, $[\omega/\sin\theta]_{cr}$. Using the assumed relative permeability relationships, the critical heat flux can be expressed as an explicit function of $\beta$:

$$[\omega/\sin\theta]_{cr} = \left(\frac{1}{1+\beta^{1/4}}\right)^4. \tag{28}$$

This critical heat flux defines the minimum dry-out condition. The maximum heat flux which can be maintained without dry-out is system dependent. For $\omega/\sin\theta$ greater than the critical value, a finite two-phase zone length ($\delta_l$) results from the integration of equation (14). If a liquid saturated layer exists above the two-phase region, dry-out will occur only if the distance from the heated surface to the liquid zone interface exceeds $\delta_l$.

## 3. EXPERIMENTAL STUDIES

Experiments were conducted using several different sand grain sizes contained in a 25.4 cm long, 5.4 cm i.d. fiberglass tube as shown in Fig. 3. Ottawa sands were chosen because of the spherical grain shape and nearly pure silica composition. The sand core was heated from the top by a nichrome wire coil imbedded in a copper block. An identical copper block heater was used to control the bottom temperature and was cooled by heat transfer to the environment. The heater temperatures were held constant through the use of two variable set point temperature controllers. Ten chromel–alumel thermocouples were placed along the sand pack centerline at 2.54 cm intervals. The core was separated from the top and bottom heaters by fired lava thermal conductivity standards in order to facilitate heat flux measurements. The core holder, standards and heaters were placed between two square steel plates, attached by four threaded rods at the corners. An axial load was applied across the section by tightening nuts on the threaded rods to ensure thermal contact between the standards and the sand pack. This load also provided a seal between the standards and the core holder separated by O-rings.

Four individually controlled heater tapes were wrapped around the core holder. Thermocouples were placed between each heater tape and the core holder on opposite sides. Individual heater tape power levels were adjusted periodically during the experiments such that the average core holder outside temperature at each of

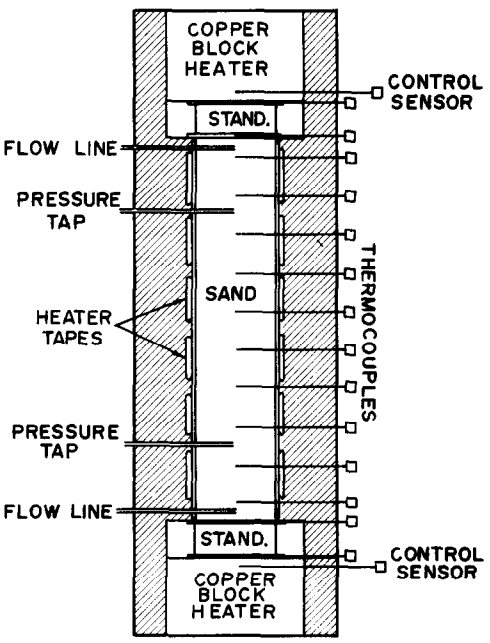


FIG. 3. Experimental apparatus.

Table 1. Summary of horizontal heating experimental results

| Experiment | Grain size ($\mu$m) | Porosity | Permeability ($m^2$) | Heat flux ($W/m^2$) | Two-phase zone length $x_1$ (m) | $\frac{qx_1\nu_v}{(\kappa\phi)^{1/2}\sigma h_{fg}}$ | Deviation from theoretical prediction (%) |
|---|---|---|---|---|---|---|---|
| 1.1 | 149–105 | 0.388 | $10.3\times10^{-12}$ | 2450 | 0.175 | 0.0325 | −12 |
| 1.2* | 149–105 | 0.388 | $10.3\times10^{-12}$ | 1975 | 0.117 | 0.0171 | −54 |
| 2.1 | 149–105 | 0.388 | $9.94\times10^{-12}$ | 1492 | 0.235 | 0.030 | −19 |
| 2.2 | 149–105 | 0.388 | $9.94\times10^{-12}$ | 1676 | 0.224 | 0.032 | −13 |
| 2.3 | 149–105 | 0.388 | $9.94\times10^{-12}$ | 2065 | 0.185 | 0.033 | −10 |
| 2.4* | 149–105 | 0.388 | $9.94\times10^{-12}$ | 1867 | 0.176 | 0.028 | −24 |

* Conducted under conditions where the two-phase zone was required to invade the vapor zone.

the four heater tape locations matched the sand pack centerline temperature. This procedure prevented radial heat flux within the sand pack and insured one-dimensional heat and mass transfer within the core holder. The one-dimensional condition was experimentally verified by measuring the heat fluxes across the top and bottom thermal conductivity standards, which matched to within 5.0% for all experiments reported.

During the packing of the core, a pneumatic vibrator was pressed to the side of the core holder to obtain a minimum porosity. The porosity was determined from the core holder volume, the mass of the sand pack and the sand grain density. Prior to each experiment, air within the core holder was removed using a vacuum pump. Distilled water was then allowed to flow into the core until the sand pack was completely saturated. Before heating, a permeability test was run. The core was then brought to saturation temperature using the top and bottom heaters as well as the heating tapes. The temperatures of the heaters were then set at predetermined levels. The fluid pressure was controlled during heating by a pressure regulator set slightly above atmospheric pressure. As the water evaporated, steam was bled off, condensed and collected in a graduated cylinder in order to obtain the average sand pack water pore volume fraction. Steady-state conditions were determined from the stabilization of all temperature and pressure data, as well as the absence of flow of steam in the bleed-off line. Cementation reported by other researchers [14], was avoided by the use of distilled water as the working fluid and by conducting all experiments on each sand pack within a span of two days to reduce the effect of silica dissolution. No evidence of cementation was observed during disassembly of the experiments.

## 4. EXPERIMENTAL RESULTS AND MODEL VERIFICATION

Experiments were conducted for the top heating and horizontal heating cases. The temperatures within the sand packs all exhibited the expected trends of linear temperature profiles in the liquid and vapor zones and a nearly isothermal transition zone separating the two end regions. For each experiment, the length of the two-phase zone was determined by extrapolating the linear temperature profiles of the single phase zones to the temperature of the transition zone. The two-phase zone length could thus be determined graphically to within 1 mm. A summary of all the experimental conditions and results are listed in Tables 1 and 2.

The data for the horizontally heated sand packs are given in Table 1 and can be compared to the theoretical wick limit given by equation (25). In all except two cases the wick limits obtained from the experiments were within 20% of the theoretical prediction. For the two runs which exceeded the 20% deviation, the

Table 2. Summary of top heating experimental results

| Experiment | Grain size: Mesh | Grain size: Dia. range ($\mu$m) | Porosity | Permeability ($m^2$) | Heat flux ($W/m^2$) | Two-phase zone length (m) | $\omega$ | $\delta_1$ |
|---|---|---|---|---|---|---|---|---|
| 4.1 | 20–28 | 833–589 | 0.33 | $1.39\times10^{-12}$ | 2260 | 0.077 | 1.52 | 0.025 |
| 4.2 | 20–28 | 833–589 | 0.33 | $1.39\times10^{-12}$ | 1660 | 0.087 | 1.12 | 0.029 |
| 5.1 | 65–100 | 208–149 | 0.38 | $6.41\times10^{-12}$* | 1900 | 0.128 | 0.282 | 0.084 |
| 5.2 | 65–100 | 208–149 | 0.38 | $6.41\times10^{-12}$* | 1510 | 0.136 | 0.224 | 0.089 |
| 5.3 | 65–100 | 208–149 | 0.38 | $6.41\times10^{-12}$* | 1520 | 0.137 | 0.226 | 0.090 |
| Su [13] | 65–100 | 208–149 | 0.38 | $6.41\times10^{-12}$ | 1210 | 0.201 | 0.180 | 0.132 |
| 6.1 | 100–200 | 149–105 | 0.39 | $9.94\times10^{-12}$ | 1010 | 0.161 | 0.097 | 0.130 |
| 6.2 | 100–200 | 149–105 | 0.39 | $9.94\times10^{-12}$ | 1434 | 0.158 | 0.138 | 0.127 |
| 6.3 | 100–200 | 149–105 | 0.39 | $9.94\times10^{-12}$ | 1546 | 0.160 | 0.148 | 0.130 |

* The permeabilities of Su [13] were assumed for identical grain sizes and porosity.

experiments were conducted in a manner requiring the two-phase zone to lengthen into the vapor zone. Instead of the expected lengthening, the interface between these two zones remained fixed in the sand pack. It is not clear why this phenomenon occurred, although one explanation seems plausible. During visualization experiments conducted on bottom heated confined sand, it was noticed that a crack in the sand pack occurred at the interface between the vapor and two-phase zones when the confining force was decreased. In fact, the entire sand pack from the two-phase zone up would behave as a piston being forced upward by the vapor pressure when the confining force was released. This same phenomena would also occur for a horizontally heated porous system if a sufficient load across the sand were not maintained. The effect of such a crack would be a capillary imbibition barrier to the liquid phase. Thus, the interface would remain fixed. Since the confining load in these experiments was borne by the core holder at the operating temperature due to a coefficient of the thermal expansion greater than that of the sand pack, it is very possible that this was the cause of the anomalies of experiments 1.2 and 2.4. This phenomenon would not be expected for top heating.

The experimental two-phase zone lengths of the top heated cases listed in Table 2 are compared in Fig. 4 to the theoretical lengths resulting from the integration of equation (14). As illustrated in this figure, excellent agreement between the theory and experiments was obtained. Also of note is that experiments 6.1 to 6.3 were conducted with a non-condensable gas present in the sand pack. The total volume of nitrogen introduced into the system was 14% of the pore volume. This quantity of non-condensable gas apparently had little effect on the system performance. Preliminary theoretical modelling work supports this conclusion.

Also shown in Fig. 4 is the theoretical prediction of the two-phase zone length for bottom heating at conditions above dry-out. The non-dimensional length becomes very large for small $\omega/\sin\theta$ near the dry-out condition, and becomes infinitely large at the dry-out condition. For large $|\omega/\sin\theta|$, both the bottom and top heating cases reduce to $\omega\delta_l = 0.0368$, the wick limit. By reference to Fig. 4, it can be concluded that gravitational effects can be neglected for $|\omega/\sin\theta| \geqslant 10$.

Although the two-phase zone lengths for high flux bottom heating could not be obtained due to limitations of the present apparatus, it was possible to record the dry-out heat flux for the sand pack of experiments 2.1–2.4. This was accomplished by incremental increases in heat flux, allowing steady state conditions to be reached at each increment. At a heat flux of 3.250 kW/m$^2$, the temperature of the bottom plate began to increase rapidly above the temperatures characteristic of the two-phase zone. The actual dry-out heat flux was between the flux given above and the flux measured at the previous increment, or $0.307 < [\omega/\sin\theta]_{cr} < 0.313$ as compared to the theoretical value of 0.303.

Data from the literature also confirms the dry-out correlation given by equation (28). The data of Bau and Torrance [14] indicate that the critical heat flux was not reached in their experiments. Under those conditions, the length of the heat pipe zone would be unbounded. Thus the conclusion of the authors that the two-phase zone lengths were determined by the total sand pack length and the thermal conductivity of the liquid zone at the top is confirmed. Data for the dry-out heat flux has been reported elsewhere [18, 25]. These values are compared to equation (28) in Fig. 5. The data from [18] shown in this figure was chosen using the criterion of $\delta_l$, based on the sample length, larger than 0.1. The data from [25] is restricted to vapor Reynolds numbers (based on the mean particle diameter and superficial velocity) less than one. As shown in the figure, good agreement between predicted and reported

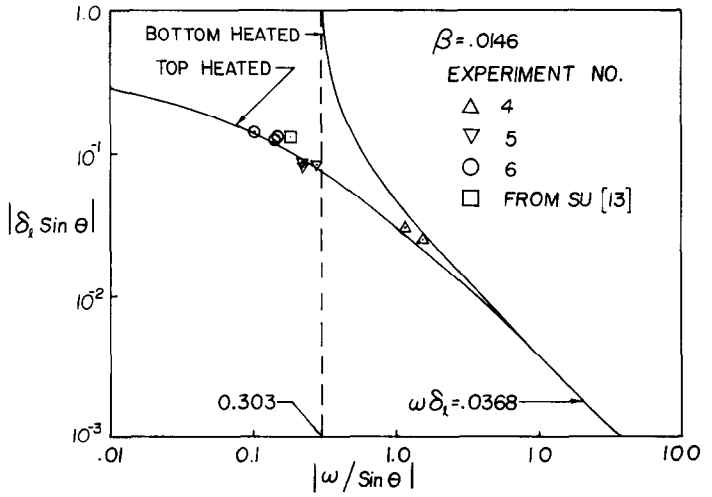


FIG. 4. Dimensionless two-phase zone lengths for water at atmospheric pressure as a function of dimensionless heat flux.

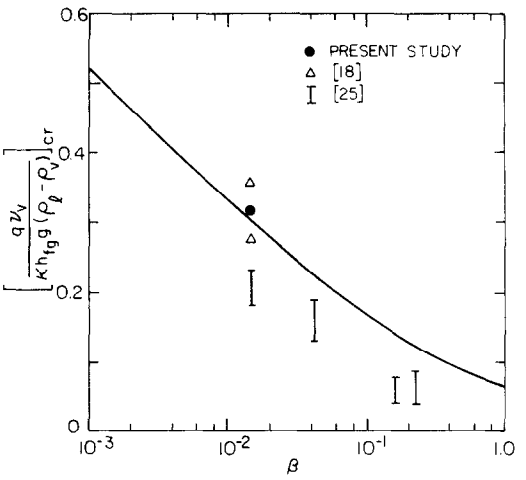


FIG. 5. Comparison of experimental data with the critical dry-out heat flux given by equation (28).

dry-out heat flux is obtained. The data given by [25] is expected to be as much as 50% low due to heat losses from those experiments. Also, most of that data was obtained near a vapor Reynolds number of one. This could account for a lower dry-out heat flux due to inertia effects.

## 5. THEORETICAL RESULTS AND DISCUSSION

Having established the accuracy and generality of the theoretical model in predicting the length of the two-phase zone and dry-out heat flux, the thermal characteristics of the two-phase region are now presented. Saturation profiles for water at atmospheric pressure are shown in Fig. 6. For the case of heating from above, the saturation gradients are larger than the horizontal heating or bottom heating cases since these gradients must provide the driving force for the liquid movement against the gravitational force. Conversely for bottom heating, the gradients are smaller since gravity assists the liquid flow. As the value of $|\omega/\sin\theta|$ becomes smaller than those of this figure, deviations from the similarity profile are increased. For bottom heating, the gradient of the saturation profile approaches zero at $s = 0.275$ as $\omega/\sin\theta \to 0.303$. The saturation profiles for the two cases with gravity effects become identical to the similarity profile as $|\omega/\sin\theta|$ becomes large.

Also of interest are the pressure profiles corresponding to these three cases. The profiles shown in Fig. 7 result from the integration of equations (17) and (18) and the boundary condition of $P_v = P_l = 0$ at $s = 1$. For all cases, it is evident that the largest vapor and liquid pressure gradients occur near the liquid zone and vapor zone boundaries, respectively. This is due to the low relative permeabilities near the endpoints. It is also of note that the normalized liquid pressures closely follow the hydrostatic pressure gradients for large values of $\delta/\delta_l$. The deviation of the horizontally heated liquid pressure from zero is indicative of the deviations from the hydrostatic pressures of the other two cases.

The temperature profiles for several different permeabilities and the three gravitational orientations are shown in Fig. 8 for a steam–water system with $T_0 = 100°C$ and a porosity of 0.40. The temperatures were found to be weakly dependent on the porosity for constant permeability. As illustrated in this figure, larger permeabilities result in smaller temperature variations within the two-phase zone. The largest temperature difference across the region occurs for the bottom heated condition, whereas the smallest temperature change corresponds to the top heating orientation. These theoretical predictions of temperature match the experimental data within the accuracy of the thermocouple readings.

The apparent thermal conductivities of the two-phase zone were calculated from the heat flux and the temperature gradients as a function of location. The

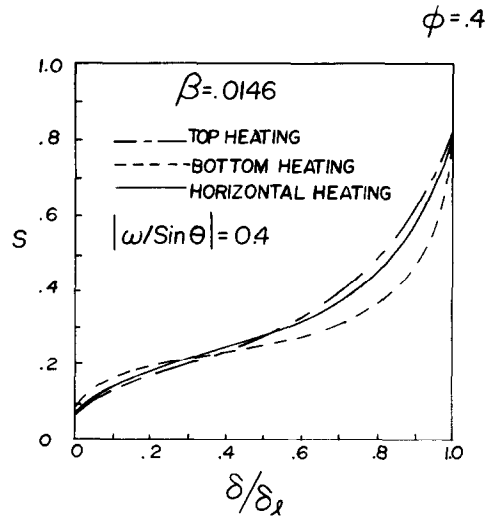


FIG. 6. Liquid saturation profiles for water saturated media with various gravitational orientations.

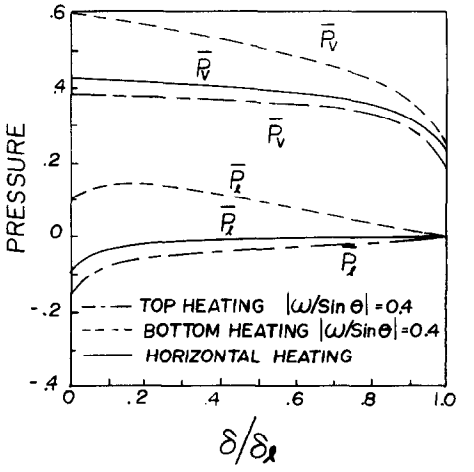


FIG. 7. Liquid and vapor pressure profiles for $\beta = 0.0146$.

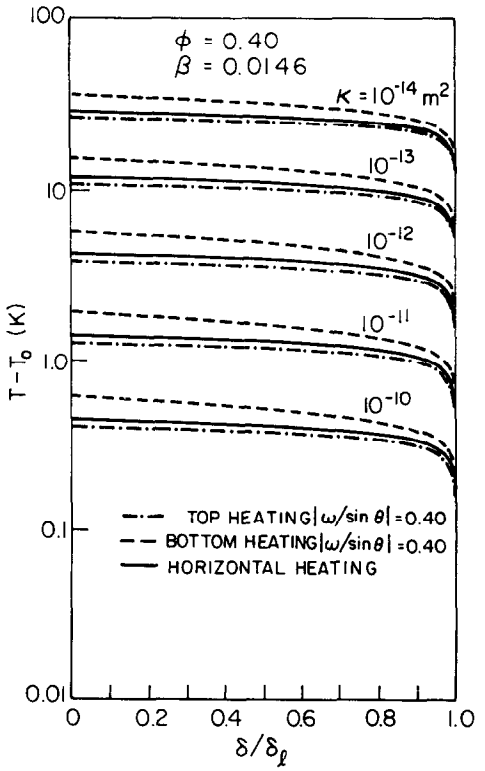


FIG. 8. Two-phase zone temperature profiles for water saturated media.

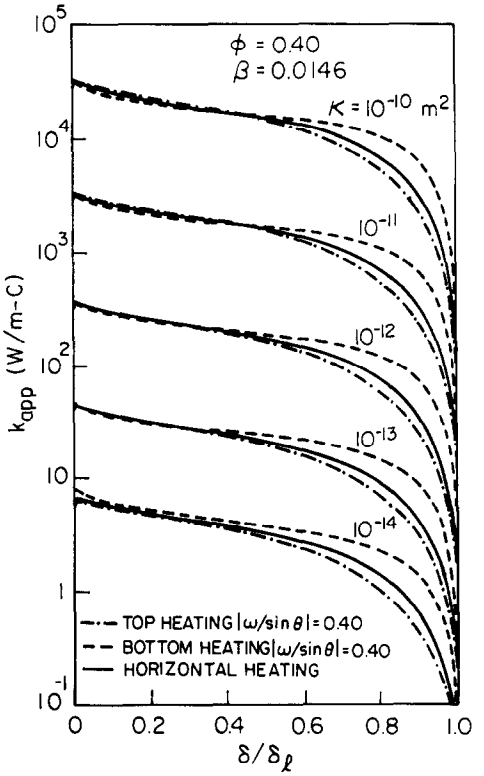


FIG. 9. Apparent thermal conductivities for water saturated media as a function of location within the two-phase zone.

results of these calculations for the three gravitational orientations are shown in Fig. 9 for several different permeabilities. The large temperature gradients near the condensing end, apparent in Fig. 8, are translated into small apparent thermal conductivities in this figure. Since the thermal conductivity of the water saturated sand used in the experiments was measured to be approximately 3 W/m K, there will be a conductive component of the overall heat transfer near the liquid zone boundary. Also, for low permeability porous media, conduction will become significant throughout the two-phase zone.

Data on the apparent thermal conductivity of experiments 2.1–2.4 can be compared to the theoretical curves shown in Fig. 9. The permeability of that sand was $9.9 \times 10^{-12}$ m$^2$ and the overall apparent thermal conductivity was 708 W/m K $\pm 9\%$. The measured conductivity falls near a curve of $\kappa = 10^{-11}$ m$^2$ and is expected to be characteristic of the conductivity near $\delta/\delta_1 = 1$ since the temperature variation in that region dominates the overall temperature difference. Thus, the model's prediction of the apparent thermal conductivities are expected to be accurate.

The extremely high apparent thermal conductivities of high permeability porous media are of major interest for various engineering applications. As illustrated in Fig. 9, these conductivities approach those of conventional heat pipes [10]. One limitation of the analysis presented in this work as applied to high permeability media which should be noted is the restriction of the vapor Reynolds number to values below one, which allows for the use of the Darcy equation. High heat fluxes may increase the vapor Reynolds number to a value above one. The inertia effects will then increase the vapor pressure gradient above that predicted by Darcy's equation, thus decreasing the effective conductivity.

Since the temperatures, pressures, and saturations within the two-phase zone are obtained from the integration of a first-order differential equation, cases where no liquid or vapor zones exist can be evaluated by simply modifying the limits of integration of equation (14). Such a case was studied by Ogniewicz and Tien [10] in order to evaluate the performance of porous heat pipes. Unfortunately, the endpoint saturations are seldom known *a priori* if a liquid or vapor zone are not present. If average liquid saturations or actual two-phase zone lengths are specified, the integration limits can be deduced through the analysis presented in this work.

In closing, it should be noted that the results obtained in this study are based on the capillary pressure and relative permeability functions specified by equations (20)–(22). The uncertainty inherent in these functions is the major source of error in this analysis. Data on countercurrent, single component, two-phase relative permeabilities do not exist to the author's knowledge. It can be postulated, however, that for countercurrent flow to occur in top and horizontal heating, both liquid and vapor phases must be continuous throughout the two-phase zone. Percolation could occur in the bottom heated case due to buoyancy forces.

## CONCLUSIONS

The theoretical analysis and experimental studies conducted in this work have produced several major results summarized below.

(1) The effect of capillarity in porous media saturated with both vapor and liquid phases of a single component fluid is the countercurrent flow of the two phases. This countercurrent flow allows for an extremely efficient heat transfer process similar to the operation of conventional heat pipes.

(2) For one-dimensional steady-state systems, the maximum length of the two-phase heat pipe zone can be obtained from the integration of the saturation gradient, equation (14). The product of the heat flux and the two-phase zone length is constant for fixed fluid and media properties under conditions of high heat fluxes or horizontally heated media. This constant is given by equation (25). The two-phase zone length will be longer for bottom heated systems and shorter if heated from above.

(3) When heated from the bottom, the two-phase zone length may be infinitely long for low heat flux. A vapor zone will occur at the heated surface only if the critical heat flux, defined by equation (28), is exceeded.

(4) The saturation profile scaled with respect to the total two-phase zone length is independent of heat flux for horizontally heated media or for $|\omega/\sin\theta| \geqslant 10$. Thus, this profile can be considered a similarity profile.

(5) The temperature difference across the two-phase zone increases with decreasing permeability, and is greatest for bottom heating and least for top heating. Both gravitational orientations reduce to the horizontally heated temperature profile for high heat flux.

(6) The effective thermal conductivity of the two-phase zone is several orders of magnitude greater than the single phase conductivity in high permeability media. For low permeability media ($\kappa \leqslant 10^{-14}$ m$^2$), conductive heat transfer will be of the same order of magnitude as the convective contribution.

*Acknowledgements*—Funding for this work was provided by the Union Oil Company, the University of California at Berkeley, and Chevron Oil Field Research. The author also wishes to acknowledge the assistance of the following students: Myron Burr, Kang-Shin Chen, Judith Jennings, Judy Hall, Kenneth Purcell, and the members of Spring 1983 Mechanical Engineering Laboratory class who participated in the experimental work. The author wishes to express thanks to Ms Loris C.-H. Donahue for typing the manuscript.

## REFERENCES

1. G. J. Boyoucos, The effect of temperature on the movement of water vapor and capillary moisture in soils, *J. Agric. Res.* **5**, 141–172 (1915).
2. H. F. Winterkorn, Fundamental similarities between electro-osmotic and thermo-osmotic phenomena, *Highway Res. Board Proc.* **27**, 443–455 (1947).
3. S. A. Taylor and L. Cavazza, The movement of soil moisture in response to temperature gradients, *Soil Sci. Soc. Am. Proc.* **18**(4), 351–365 (1954).
4. J. R. Philip and D. A. DeVries, Moisture movement in porous material under temperature gradients, *Trans. Am. Geophys. Union* **38**, 222 (1957).
5. A. V. Luikov, Systems of differential equations of heat and mass transfer in capillary-porous bodies, *Int. J. Heat Mass Transfer* **18**, 1–14 (1975).
6. O. Krischer, *Die wissenschaftlichen Grundlagen der Trocknungstechnik*, Springer, Berlin (1963).
7. M. S. Sahota and P. J. Pagni, Heat and mass transfer in porous media subject to fires, *Int. J. Heat Mass Transfer* **22**, 1069–1081 (1979).
8. E. R. G. Eckert and M. Faghri, A general analysis of moisture migration caused by temperature differences in an unsaturated porous medium, *Int. J. Heat Mass Transfer* **23**, 1613–1623 (1980).
9. Y. Ogniewicz and C. L. Tien, Analysis of condensation in porous insulation, *Int. J. Heat Mass Transfer* **24**, 421–429 (1981).
10. Y. Ogniewicz and C. L. Tien, Porous heat pipe, Paper 79-1093, AIAA 14th Thermophysics Conference, Orlando, Florida, June (1979).
11. D. Hansen, W. H. Breyer and W. J. Riback, Steady state heat transfer in partially liquid filled porous media, *J. Heat Transfer* **92**(3), 520–527 (1970).
12. E. E. Gomma and W. H. Somerton, The behavior of multifluid-saturated formations, Part II: Effect of vapor saturation—heat pipe concept and apparent, thermal conductivity, SPE Paper 4896-B, *Proc. Soc. Petroleum Engineers California Regional Meeting*, San Francisco, April (1974).
13. H. J. Su, Heat transfer in porous media with fluid phase change, Ph.D. thesis, University of California, Berkeley (1981).
14. H. H. Bau and K. E. Torrance, Boiling in low-permeability porous materials, *Int. J. Heat Mass Transfer* **25**(1), 45–55 (1982).
15. C. H. Sondergeld and D. L. Turcotte, An experimental study of two-phase convection in a porous medium with applications to geological problems, *J. Geophys. Res.* **82**(14), 2045–2053 (1977).
16. T. Abe, E. R. G. Eckert and R. J. Goldstein, A parametric study of boiling in a porous bed, *Wärme- und Stoffübertragung* **16**, 119–126 (1982).
17. V. Dhir and I. Catton, Dryout heat fluxes for inductively heated particulate beds, *J. Heat Transfer* **99**, 250–256 (1977).
18. J. K. Ferrell and J. Alleavitch, Vaporization heat transfer in capillary wick structures, *Chem. Engng. Prog. Symp., Ser. No. 102*, **66**, 82–91 (1970).
19. R. A. Moss and A. J. Kelly, Neutron radiographic study of limiting planar heat pipe performance, *Int. J. Heat Mass Transfer* **13**, 491–502 (1970).
20. K. Cornwell, B. G. Nair and T. D. Patten, Observation of boiling in porous media, *Int. J. Heat and Mass Transfer* **19**, 236–238 (1976).
21. K. S. Udell, Heat transfer in porous media heated from above with evaporation, condensation and capillary effects, *J. Heat Transfer* **105**(3), 485–492 (1983).
22. M. C. Leverett, Capillary behavior in porous solids, *AIME Trans.* **142**, 152–169 (1941).
23. I. Fatt and W. A. Klikoff, Effect of fractional wettability on multiphase flow through porous media, AIME Technical Note No. 2043, *AIME Trans.* **216**, 246 (1959).
24. M. R. J. Wyllie, Relative permeability, in *Petroleum Production Handbook* (edited by Frick), Vol. 2, Ch. 25, McGraw-Hill, New York (1962).
25. S. W. Jones, A study of dryout heat fluxes, Ph.D. thesis, Northwestern University, Evanston, Ill. 1982.

## TRANSFERT THERMIQUE DANS UN MILIEU POREUX EN CONSIDERANT LE CHANGEMENT DE PHASE ET L'EFFET DE CAPILLARITE PAR CALODUC

**Résumé**—On considère l'analyse monodimensionnelle, premanente du transfert de chaleur et de masse dans des milieux poreux saturés par les phases liquide et vapeur d'un fluide à composant unique. On inclut les effets des forces de capillarité, de gravité et le changement de phase. Des résultats théoriques sont comparés avec un excellent accord aux données expérimentales. On trouve que le transfert thermique est augmenté de plusieurs ordres de grandeur par rapport à la conduction pure due à l'évaporation, le convection et la condensation, phénomène semblable à l'opération conventionnelle dans un caloduc. Le flux thermique d'assèchement est estimé et vérifié pour l'orientation de chauffage de la base. On obtient des profils de température, de pression et de saturation dans la région diphasique. Des conductivités thermiques apparentes sont évaluées pour différentes orientations gravitationnelles et perméabilités.

## WÄRMEÜBERTRAGUNG IN PORÖSEN MEDIEN UNTER BERÜCKSICHTIGUNG VON PHASENÄNDERUNG UND KAPILLARWIRKUNG—DER 'HEAT-PIPE'-EFFEKT

**Zusammenfassung**—Eine eindimensionale stationäre Analyse der Wärme- und Stoffübertragung in einem porösen Medium, das mit Flüssigkeit und Dampf eines reinen Fluides gesättigt ist, wurde durchgeführt. Dabei wurden Kapillar- und Schwerkraft sowie Phasenänderungseffekte berücksichtigt. Die theoretischen Ergebnisse wurden mit Versuchsdaten verglichen, wobei sich vorzügliche Übereinstimmung ergab. Es zeigte sich, daß der Wärmetransport infolge von Verdampfung, Konvektion und Kondensation um einige Größenordnungen im Vergleich zur reinen Wärmeleitung verbessert wird, wie man das auch von konventionellen Wärmerohren her kennt. Die Wärmestromdichte, bei der 'dryout' auftritt, wurde für den Fall berechnet und experimentell bestätigt, daß die Anordnung von unten her beheizt wird. Es ergaben sich die theoretischen Profile für Temperatur, Druck und Ort der Sättigung im Zweiphasen-Gebiet. Für verschiedene Orientierungen bezüglich des Schwerkraftvektors und unterschiedliche Permeabilitäten des Mediums wurden scheinbare Wärmeleitfähigkeiten berechnet.

## ТЕПЛОПЕРЕНОС В ПОРИСТЫХ СРЕДАХ С УЧЕТОМ ФАЗОВОГО ПЕРЕХОДА И КАПИЛЛЯРНОСТИ. ЭФФЕКТ ТЕПЛОВОЙ ТРУБЫ

**Аннотация**—Проведен одномерный стационарный анализ тепло- и массопереноса в пористых средах, насыщенных жидкой и паровой фазами однокомпонентной жидкости. Рассматривались эффекты капиллярности, сил тяжести и фазового превращения. Получено хорошее совпадение теоретических результатов с экспериментальными данными. Найдено, что теплоперенос возрастает на несколько порядков за счет испарения, конвекции и конденсации, аналогично тому, как это происходит в обычной тепловой трубе. Рассчитана величина критического теплового потока и проведена ее проверка при нагреве снизу. Теоретически получены профили температуры, давления и насыщения внутри двухфазной области. Дана оценки коэффициентов кажущейся теплопроводности при различных значениях проницаемости среды и ориентации силы тяжести.